Aerospace Science and Technology 91 (2019) 12–27

Contents lists available at ScienceDirect

Aerospace Science and Technology

www.elsevier.com/locate/aescte

# Neural network-based adaptive sliding mode control design for position and attitude control of a quadrotor UAV

Hadi Razmi [a,*], Sima Afshinfar [b]

[a] Department of Electrical Engineering, East Tehran Branch, Islamic Azad University, Tehran, Iran
[b] Young Researchers and Elite club, East Tehran Branch, Islamic Azad University, Tehran, Iran

ARTICLE INFO

*Article history:*
Received 16 May 2018
Received in revised form 16 December 2018
Accepted 30 April 2019
Available online 7 May 2019

*Keywords:*
Sliding mode control
Neural network
Quadrotor

ABSTRACT

In this paper, a novel method is suggested for the position and attitude tracking control of a quadrotor UAV in the presence of parametric uncertainties and external disturbance. The proposed method combines neural network adaptive scheme with sliding mode control, which preserves the advantages of the two methods. Firstly, dynamic model of quadrotor is divided into two fully actuated and under actuated subsystems. Secondly, sliding mode controllers are corresponding designed for each subsystem, and their coefficients in sliding manifolds are adaptively tuned by the neural network method. In each section, using Lyapunov theory, stability of closed loop system is proven.
Finally, the method is examined for a square path tracking and a maximum overshoot of 7.5133% and a settling time 5.6648 s are obtained. By comparing the results obtained through different methods, it is concluded that the proposed controller provides the following main advantages: (1) good transient and steady state behaviors, (2) insensitivity to parameter variations, (3) disturbance rejection capability, and (4) remarkable stability and performance robustness. Hence, for operational purposes in which the fast and accurate response are of crucial importance, using the neural network-based adaptive sliding mode control approach is recommended.



## 1. Introduction

More recently, Unmanned Aerial Vehicles (UAVs) such as quadrotors are an important part of scientific studies in the fields of commercial military, civilian, industrial, and academic platform [1,2]. The quadrotors have a lot of benefits such as the Vertical Take-Off and Landing (VTOL), hover capability, high speed maneuverability, good agility, small size, light weight, low cost, and high performance [3,4]. Due to these benefits, their applications domains cover photography, mapping, monitoring, inspection, reconnaissance, surveillance, search and rescue, and remote inspection [3,5].

However, the control of a quadrotor is difficult because of the highly coupled nonlinear dynamics, unstable and multi-variable nature, possibly non-minimum phase, underactuation, as well as existence parameter uncertainties and external disturbances, like payload, wind gusts, model uncertainties, and internal friction [6].

So far, different methods for attitude and position control of the quadrotor, such as linear control, nonlinear control, optimal control, adaptive control, robust control and intelligent control methods, have been proposed in the literature [7,8], and some of them have been reviewed in [9]. Sliding mode control method is one of the most useful and efficient approaches used to control the quadrotor because of the fast response, good transient performance, easy tuning and implementation, and strong robustness with respect to bounded external disturbances and system uncertainties [10].

A pure sliding mode controller has the following challenges and drawbacks in practical applications:

- Chattering problem or high frequency oscillations of the control signals,
- Stability analysis,
- Tracking performance in finite time,
- High vulnerability to measurement noise,
- Employment of unnecessarily large control signals to overcome the parametric uncertainties,
- Necessity of a thorough and accurate knowledge of the plant dynamics for the calculation of the equivalent control.

* Corresponding author.
*E-mail addresses:* razmi.hadi@gmail.com (H. Razmi), simaafshinfar@gmail.com (S. Afshinfar).

https://doi.org/10.1016/j.ast.2019.04.055
1270-9638/

**Nomenclature**

| | |
|---|---|
| $[\theta, \phi, \psi]^T$ | The orientation angle vector of the quadrotor in body-frame |
| $[x, y, z]^T$ | The position vector of the center of the gravity of the quadrotor in earth-frame |
| $\Omega_i$ $(i = 1, \cdots, 4)$ | The angular speed of the propeller $i$ |
| $\Omega_r$ | The overall residual rotor angular velocity |
| $C$ | The force to moment scaling factor |
| $g$ | The acceleration of gravity |
| $I_x$, $I_y$, and $I_z$ | The mass moments of inertia in the $x$, $y$, and $z$ axes, respectively |
| $J_r$ | The inertia of the propeller |
| $k_i$ $(i = 1, \cdots, 6)$ | The drag coefficients |
| $l$ | The distance from the center of each rotor to the center of the gravity of the quadrotor |
| $m_s$ | The total mass of the quadrotor |
| UAV | Unmanned Aerial Vehicle |
| VTOL | Vertical Take-Off and Landing |

Therefore, in order to overcome one or more of these drawbacks, many modifications to the classical sliding mode control have been suggested in the literature.

In [8] an adaptive sliding mode control is suggested for finite-time stabilization of quad-rotor unmanned aerial vehicle in face of parametric uncertainties. A second order sliding mode control for the position and attitude tracking control of a small quadrotor UAV is suggested in [11]. In [12], an adaptive fuzzy gain-scheduling sliding mode method is proposed for the attitude control of quadrotors in the presence of parametric uncertainties and external disturbances. A global fast dynamic terminal sliding mode control scheme is designed in [13] for the finite-time position and attitude tracking control of a small quadrotor UAV with external disturbances. In [14], a novel robust terminal sliding mode controller and a sliding mode controller are recommended for position and attitude tracking of the fully actuated and underactuated subsystems of a small quadrotor unmanned aerial vehicle, respectively. In [15], a new control structure that employs the least squares method to solve the over-determined problem of the control input in the translational motion and the sliding mode controller is suggested to provide robust tracking and stabilization of a quadcopter. The reference [16] presents a chattering free adaptive integral sliding mode controller for stabilizing a class of multi-input multi-output systems under both matched and mismatched types of uncertainties. Stabilization of the vertical take-off and landing aircraft system is considered to demonstrate the effectiveness of the proposed controller. In [17], a fault-tolerant neural network interval type-2 fuzzy sliding mode trajectory tracking controller is proposed for each subsystem of the octorotor helicopter in the presence of actuator and sensor faults. The reference [18] presents a control strategy based on interval fuzzy type-2 and sliding mode for attitude and position tracking problem of a coaxial trirotor in the presence of defects in the system. In [19], three second order sliding mode control methods, i.e., the super twisting sliding mode controller, the modified super twisting sliding mode controller and the nonsingular terminal super twisting sliding mode controller are employed for the altitude tracking of a quadrotor aircraft in a real-time application at outdoors environments. In [20], the design of position and attitude tracing controllers based on the adaptive radical basis function neural networks and double-loop integral sliding mode control for a quadrotor unmanned aerial vehicle is addressed in the presence of sustained disturbances and parameter uncertainties. The authors in [21] developed a robust chattering-free altitude controller based on a continuous sliding mode control for the efficient performance of a quadrotor aircraft system. The integral sliding mode controller based on backstepping is proposed in [22] for the underactuated model of a quadrotor subject to smooth bounded disturbances, including sideslip aerodynamics and wind gust, as well as dissipative drag in orientation and position dynamics. In [23] a novel robust terminal sliding mode controller combined with an under-actuated system sliding mode controller is used to control the attitude of a small quad-rotor unmanned helicopter in the presence of external disturbances. The authors in [24] proposed the sliding mode control technique combined with the backstepping control technique for a quadrotor unmanned aerial vehicle in order to achieve Cartesian position trajectory tracking capability.

From the literature survey, the main challenge with the sliding mode control is found in the tuning of its sliding surface parameters. The sliding mode control can be investigated in two parts. The reaching or hitting phase is the first part where the trajectories starting from a given initial condition and move toward the sliding surface. During this phase, the system response is sensitive to parameter variations and disturbances and cannot be controlled directly. The second part is known as the sliding phase. During this phase, the trajectories move only on the desired sliding surface and are insensitive to parameter variations and noise. Therefore, various methods have been introduced to shorten the duration or even eliminate the reaching phase. In order to meet this goal and improving the performance of the system with sliding mode control algorithms, time-varying switching surfaces instead of constant surfaces has been used in the literature [25]. In [26], a neural-network-based adaptive gain scheduling backstepping sliding mode control approach is recommended for a class of uncertain strict-feedback nonlinear system. Chattering phenomenon as a common problem in the SMC is reduced by employing a radial basis function neural network in this reference. In [27], a new control structure employing fuzzy adaptive sliding mode control is suggested for trajectory tracking of an autonomous airship to provide robust tracking in the presence of model uncertainties. In [28], a neural network approximation-based nonsingular terminal sliding mode controller is proposed for trajectory tracking of robotic airships. In order to meet the lump uncertainties of the robotic airship, the radical basic function neural network is employed. In [29], a novel time specified nonsingular terminal sliding mode control scheme is proposed for trajectory tracking of robotic airships. In order to guarantee the specified finite time stability, a nonsingular terminal sliding manifold is employed in this paper.

Neural networks, one of the most popular intelligent computation approaches, which have powerful capability of tackling nonlinearity, fault tolerance, adaptation, generalization, and continuously online learning [30], are good candidates for this purpose. Thus, an adaptive sliding surface based on neural networks, which has not been investigated so far, will be studied.

This paper studies the position and attitude control problem for a quadrotor UAV in the presence of parametric uncertainties and external disturbances and proposes an adaptive robust controller based on the sliding mode control technique combined with the neural network scheme. The designed controller is divided into four sub-controllers: altitude controller, yaw angle controller, pitch angle controller, and roll angle controller. The sliding surface coefficients in each of these controllers are adaptively tuned by the neural network method. The stability of closed loop system is proven by the Lyapunov theory. Simulation results are presented to

demonstrate the effectiveness of the offered technique compared to the previous methods in different situations. The main contributions of this paper are as follows:

- A novel method is suggested for the position and attitude tracking control of a quadrotor UAV in the presence of parametric uncertainties and external disturbance, which preserves the advantages of the sliding mode control method and the neural network adaptive scheme.
- Instead of using the general learning method, the specialized learning method have been used to train the neural network. With this learning architecture, there is no longer a specific training phase, and the neural network is trained online. The specialized learning architecture is "goal-directed" and back-propagation adaptively adjusts the sliding mode controller parameters at every sample so that the actual plant output approaches the desired output.
- An adaptive tuning sliding surface is considered for reducing the duration of the reaching phase, ensuring less sensitivity to parameter variations and disturbances.
- The time-varying switching surfaces with the hyperbolic tangent function in definition is used in order to prevent the occurrence of the chattering phenomenon in the control inputs.
- Combining the neural networks with sliding mode controllers, results in a better tracking performance compared to the results presented in the references [11] and [13], in terms of settling time, maximum overshoot, and steady state error.

This article consists of the following sections:

In the second section, mathematical modeling of the quadrotor is presented. In the third section, problem statement is addressed. In the fourth section, the details of controller design are expressed. The simulation and comparison results are provided in the fifth section. In the sixth section, the conclusions are presented.

## 2. Mathematical modeling

The quadrotor UAV is a six degrees of freedom aircraft with four rotors arranged in a cross shape. The dynamic equations of the quadrotor by definition of body-frame and earth-frame are as follows [11,13]:

$$\ddot{x} = \frac{\sin\theta\cos\phi\cos\psi + \sin\phi\sin\psi}{m_s}u_1 - \frac{k_1\dot{x}}{m_s} \tag{1}$$

$$\ddot{y} = \frac{\sin\theta\cos\phi\sin\psi + \sin\phi\cos\psi}{m_s}u_1 - \frac{k_2\dot{y}}{m_s} \tag{2}$$

$$\ddot{z} = \frac{\cos\theta\cos\phi}{m_s}u_1 - g - \frac{k_3\dot{z}}{m_s} \tag{3}$$

$$\ddot{\phi} = \dot{\theta}\dot{\psi}\frac{I_y - I_z}{I_x} + \frac{J_r}{I_x}\dot{\theta}\Omega_r + \frac{l}{I_x}u_2 - \frac{k_4 l}{I_x}\dot{\phi} \tag{4}$$

$$\ddot{\theta} = \dot{\phi}\dot{\psi}\frac{I_z - I_x}{I_y} - \frac{J_r}{I_y}\dot{\phi}\Omega_r + \frac{l}{I_y}u_3 - \frac{k_5 l}{I_y}\dot{\theta} \tag{5}$$

$$\ddot{\psi} = \dot{\theta}\dot{\phi}\frac{I_x - I_y}{I_z} + \frac{c}{I_z}u_4 - \frac{k_6}{I_z}\dot{\psi} \tag{6}$$

For the quadrotor dynamic model given by (1)–(6), the following assumptions are made [11]:

- The angular velocity of the quadrotor in earth-frame and body-frame are the same when the quadrotor is hovering in the air.
- The quadrotor structure is symmetric and rigid.
- The origin of the body-frame and the center of gravity is one.
- The axes of the body-frame are coincident to the quadrotor inertia axes.

It should be noted that the roll, pitch and yaw angles are limited to $(-\frac{\pi}{2} < \phi < \frac{\pi}{2})$, $(-\frac{\pi}{2} < \theta < \frac{\pi}{2})$ and $(-\pi < \psi < \pi)$, respectively [11].

Also, control inputs $u_1$, $u_2$, $u_3$ and $u_4$ can be calculated by the following equation [11]:

$$\begin{pmatrix} u_1 \\ u_2 \\ u_3 \\ u_4 \end{pmatrix} = \begin{pmatrix} b & b & b & b \\ lb & 0 & -lb & 0 \\ 0 & -lb & 0 & lb \\ -k & k & -k & k \end{pmatrix} \begin{pmatrix} \Omega_1^2 \\ \Omega_2^2 \\ \Omega_3^2 \\ \Omega_4^2 \end{pmatrix} \tag{7}$$

where, $k$ and $b$ are two positive constant parameters whose values depend on the number of blades, the lift and drag coefficients of the blade, the radius of the propeller, the geometry, and the density of air [11].

## 3. Problem statement

Differential equations of the quadrotor can be introduced as the following compact affine nonlinear state space form:

$$\begin{cases} \dot{x}_i = x_{i+1} \\ \dot{x}_{i+1} = f(\boldsymbol{x}) + h(\boldsymbol{x})u_j + d(\boldsymbol{x}) \end{cases} \tag{8}$$

where, $\boldsymbol{x} = [x_1, \ldots, x_i, x_{i+1}, \ldots, x_{12}]^T = [x, \dot{x}, y, \dot{y}, z, \dot{z}, \phi, \dot{\phi}, \theta, \dot{\theta}, \psi, \dot{\psi}]^T$ is the system state vector, $u_j$ is one of the control inputs $\{u_1, u_2, u_3, u_4\}$, and $f(\boldsymbol{x})$ and $h(\boldsymbol{x}) \neq 0$ are two smooth non-linear, real and known functions of $\boldsymbol{x}$.

The trajectory tracking control objective can be stated as follows:

On the basis of $x_i$, given a desired $x_{id}$, determines piecewise continuous control law $u_j$ for the quadrotor which is function of state variables only and achieves desirable tracking performance in the presence of parametric uncertainties in $f(\boldsymbol{x})$ and $h(\boldsymbol{x})$ and unknown time-varying disturbances $d(\boldsymbol{x})$, with all state variables stabilized.

**Assumption 1.** $d(\boldsymbol{x})$, which represents the disturbances and the uncertainties, will be ignored in controller design as not modeled dynamic term.

**Assumption 2.** The desired trajectory $x_{id}$ and the first and second order derivatives of $x_{id}$ are bounded and measurable.

## 4. Controller design

The dynamic model of the quadrotor can be divided into the following subsystems:

- A fully-actuated subsystem.
- An under-actuated subsystem.

Altitude and yaw angle controllers will be designed for the fully-actuated subsystem as well as pitch and roll angles controllers for the under-actuated subsystem. Fig. 1 shows the block diagram of these controllers. In this research work, a novel adaptive sliding mode controller based on neural networks is used for the position and attitude control of the quadrotor, which is described in details, in the following subsections.

### 4.1. Altitude controller design

The altitude controller must be designed in a way that the state variable $z$ can track the desired path $z_d$. According to (8), the dynamic equation (3) can be rewritten as follows:

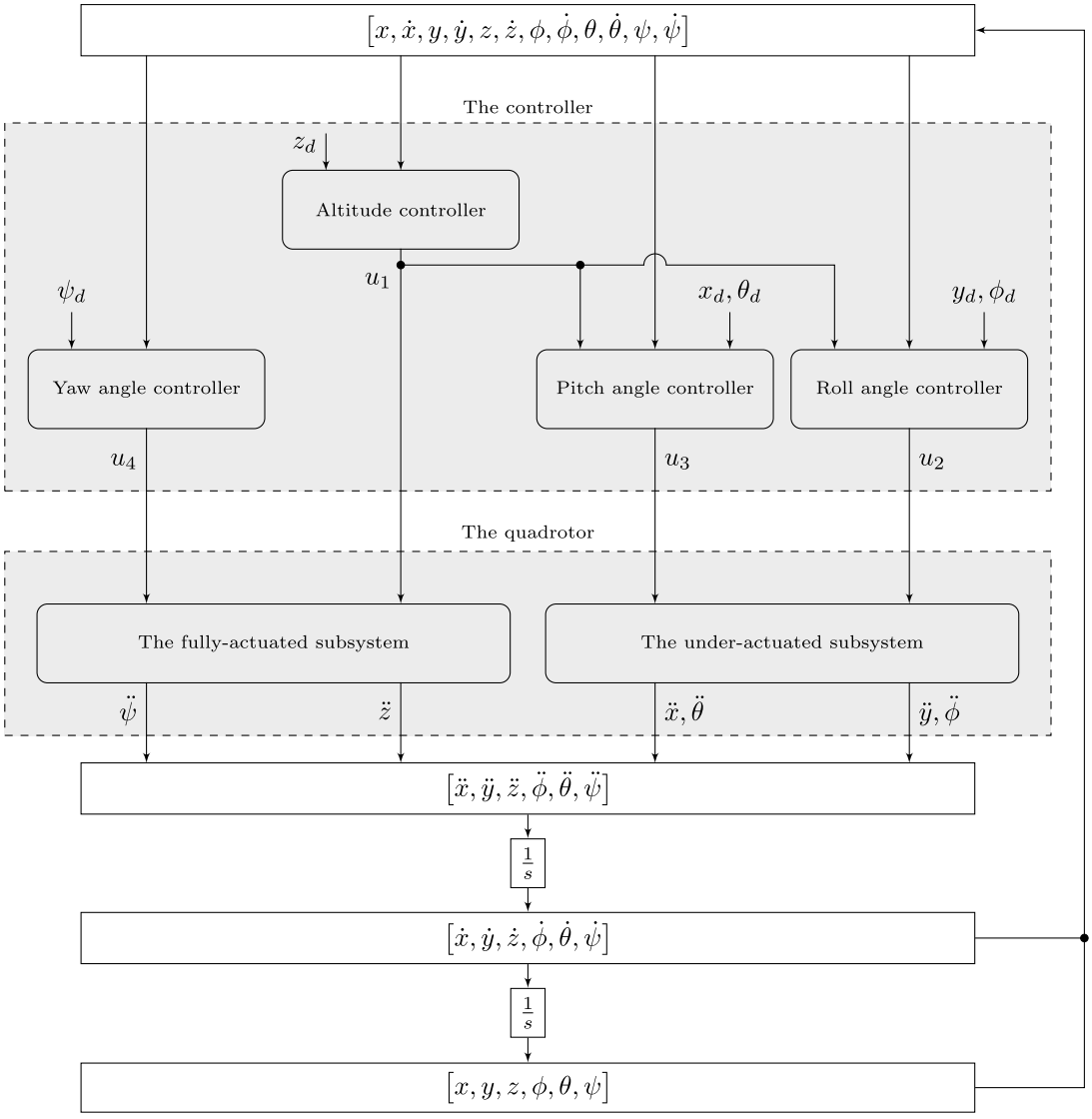


**Fig. 1.** The control block diagram.

$$\begin{cases} \dot{x}_5 = x_6 \\ \dot{x}_6 = [-g] + [\frac{\cos\theta\cos\phi}{m_s}]u_1 + [-\frac{k_3\dot{z}}{m_s}] \end{cases} \tag{9}$$

where, $i = 5$, $j = 1$, $x_5 = z$, $x_6 = \dot{z}$, $f(\boldsymbol{x}) = -g$, $h(\boldsymbol{x}) = \frac{\cos\theta\cos\phi}{m_s}$, and $d(\boldsymbol{x}) = -\frac{k_3\dot{z}}{m_s}$. Altitude control algorithm structure of the quadrotor is shown in Fig. 2 which is described as the following steps:

**Step 1.** Select the sliding surface as follows:

$$s_z = w_z(z_d - z) + (\dot{z}_d - \dot{z}) \tag{10}$$

where, $w_z$ is a design positive constant.

The differential of $s_z$ is:

$$\dot{s}_z = w_z(\dot{z}_d - \dot{z}) + (\ddot{z}_d - \ddot{z}) \tag{11}$$

Substituting (3) into (11) yields:

$$s_z = w_z(\dot{z}_d - \dot{z}) + \ddot{z}_d - \frac{\cos\theta\cos\phi}{m_s}u_1 + g \tag{12}$$

**Remark 1.** It is clear that selecting a positive number for $w_z$, provides the desired asymptotic behavior in steady state.

**Step 2.** Define the reaching law as follows:

$$\dot{s}_z = -\varepsilon_z \tanh s_z \tag{13}$$

where, $\varepsilon_z$ is a designed positive number.

**Step 3.** With the consideration of (12) and (13), the control law $u_1$ is designed as follows:

$$u_1 = \underbrace{\frac{m_s}{\cos\theta\cos\phi}[w_z(\dot{z}_d - \dot{z}) + \ddot{z}_d + g]}_{u_{1eq}} + \underbrace{\frac{m_s}{\cos\theta\cos\phi}[\varepsilon_z \tanh s_z]}_{u_{1dis}} \tag{14}$$

The control law $u_1$ have two terms, namely the equivalent control term $u_{1eq}$ and discontinuous control term $u_{1dis}$.

**Remark 2.** In order to take the system towards the designed sliding surface regardless of the sign of the states, and to eliminate the chattering phenomenon caused by the switching control action, the hyperbolic tangent function is used to design the discontinuous control $u_{1dis}$.

**Step 4.** The stability of the closed-loop system is proven as follows:

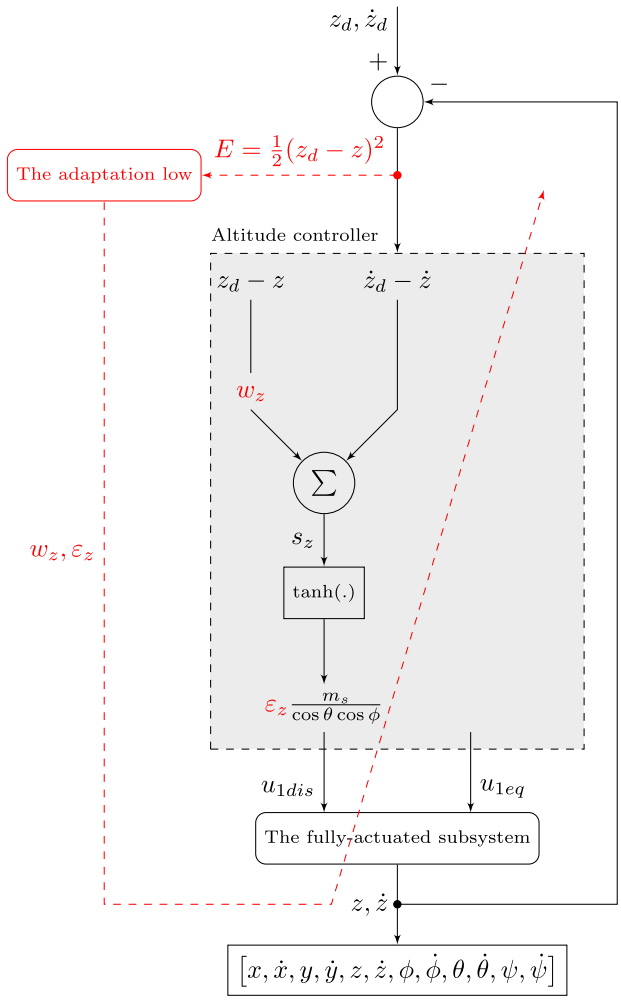


**Fig. 2.** The altitude controller block diagram. (For interpretation of the colors in the figure(s), the reader is referred to the web version of this article.)

**Theorem 1.** *For the nonlinear system (9), if the sliding surface $s_z$ is selected as (10), and the control law $u_1$ is designed as (14), then the close-loop system will be stable, and it can guarantee the state errors converge to zero.*

**Proof.** Select the following positive Lyapunov function candidate:

$$V = \frac{1}{2}s_z^2 \tag{15}$$

Invoking (13), the time derivative of $V$ is:

$$\dot{V} = \dot{s}_z s_z = -\varepsilon_z s_z \tanh s_z \leq -\varepsilon_z |s_z| \leq 0 \tag{16}$$

From (16), it is concluded that $\dot{V}$ will always be negative and the $u_1$ designed as (14) ensures Lyapunov stability of the nonlinear system (9). Therefore, the Theorem 1 has been verified. □

**Remark 3.** There are two parameters which need to be designed for sliding surface (10) and discontinuous control (14), $w_z$ and $\varepsilon_z$. These parameters can be determined based on the requirements for the steady-state tracking precision or the fastness of the sliding mode system and the conversion speed of discontinuous control.

**Step 5.** Neural network is deployed to adjust the coefficients $w_z$ and $\varepsilon_z$ with the adaptation law derived from the conventional back propagation algorithm. The neural network is trained by the specialized learning architecture [31] to minimize the following performance error $E$ which is defined as a function of the difference between the actual plant output and the desired output:

$$E = \frac{1}{2}(z_d - z)^2 \tag{17}$$

Invoking the gradient descent method [32], we have the following adaptation equations:

$$\varepsilon_z = \varepsilon_{z,0} - \eta_z \int_0^t \frac{\partial E}{\partial \varepsilon_z} dt \tag{18}$$

$$w_z = w_{z,0} - \eta_z \int_0^t \frac{\partial E}{\partial w_z} dt \tag{19}$$

where, $\eta_z$ is the learning rate which determines the convergence speed of neural network, and $\varepsilon_{z,0}$ and $w_{z,0}$ are the initial values of $\varepsilon_z$ and $w_z$, respectively.

Using the chain rule, $\frac{\partial E}{\partial \varepsilon_z}$ and $\frac{\partial E}{\partial w_z}$ are obtained as follows:

$$\frac{\partial E}{\partial \varepsilon_z} = \frac{\partial E}{\partial z}\frac{\partial z}{\partial u_{1dis}}\frac{\partial u_{1dis}}{\partial \varepsilon_z} = -(z_d - z)\frac{\partial z}{\partial u_{1dis}}\frac{m_s \tanh s_z}{\cos\theta\cos\phi} \tag{20}$$

$$\begin{aligned}\frac{\partial E}{\partial w_z} &= \frac{\partial E}{\partial z}\frac{\partial z}{\partial u_{1dis}}\frac{\partial u_{1dis}}{\partial s_z}\frac{\partial s_z}{\partial w_z} \\ &= -(z_d - z)\frac{\partial z}{\partial u_{1dis}}\frac{m_s \varepsilon_z}{\cos\theta\cos\phi}\frac{4e^{-2s_z}}{(1+e^{-2s_z})^2}(z_d - z)\end{aligned} \tag{21}$$

Assuming $\frac{\partial z}{\partial u_{1dis}} = \text{sign}\left(\frac{\nabla z}{\nabla u_{1dis}}\right)$ [33,34], we have:

$$\varepsilon_z = \varepsilon_{z,0} + \eta_z \int_0^t \text{sign}\left(\frac{\nabla z}{\nabla u_{1dis}}\right)\frac{m_s(z_d - z)\tanh s_z}{\cos\theta\cos\phi} dt \tag{22}$$

$$w_z = w_{z,0} + \eta_z \int_0^t \text{sign}\left(\frac{\nabla z}{\nabla u_{1dis}}\right)\frac{4m_s\varepsilon_z(z_d - z)^2 e^{-2s_z}}{\cos\theta\cos\phi(1+e^{-2s_z})^2} dt \tag{23}$$

where, $\nabla$ is called the ascending or backward differences operator, as $\nabla f_k = f_k - f_{k-1}$.

**Assumption 3.** The parameters $\eta_z$, $\varepsilon_{z0}$, and $w_{z0}$ in (22) and (23) will be determined by the trial and error method.

### 4.2. Yaw angle controller design

The yaw angle controller must be designed so that the state variable $\psi$ can track the desirable path $\psi_d$. Invoking (6) and (8), dynamical equations required for this subsystem can be rewritten as follows:

$$\begin{cases}\dot{x}_{11} = x_{12} \\ \dot{x}_{12} = [0] + [\frac{c}{I_z}]u_4 + [-\frac{k_6}{I_z}\dot{\psi}]\end{cases} \tag{24}$$

where, $i = 11$, $j = 4$, $x_{11} = \psi$, $x_{12} = \dot{\psi}$, $f(\boldsymbol{x}) = 0$, $h(\boldsymbol{x}) = \frac{c}{I_z}$, and $d(\boldsymbol{x}) = -\frac{k_6}{I_z}\dot{\psi}$.

**Remark 4.** Due to the fact that the structure of the quadrotor and its rotors are considered rigid and symmetric, so $I_x = I_y$.

Similar to the altitude control algorithm structure, the sliding surface $s_\psi$ and control input $u_4$ are designed as follows:

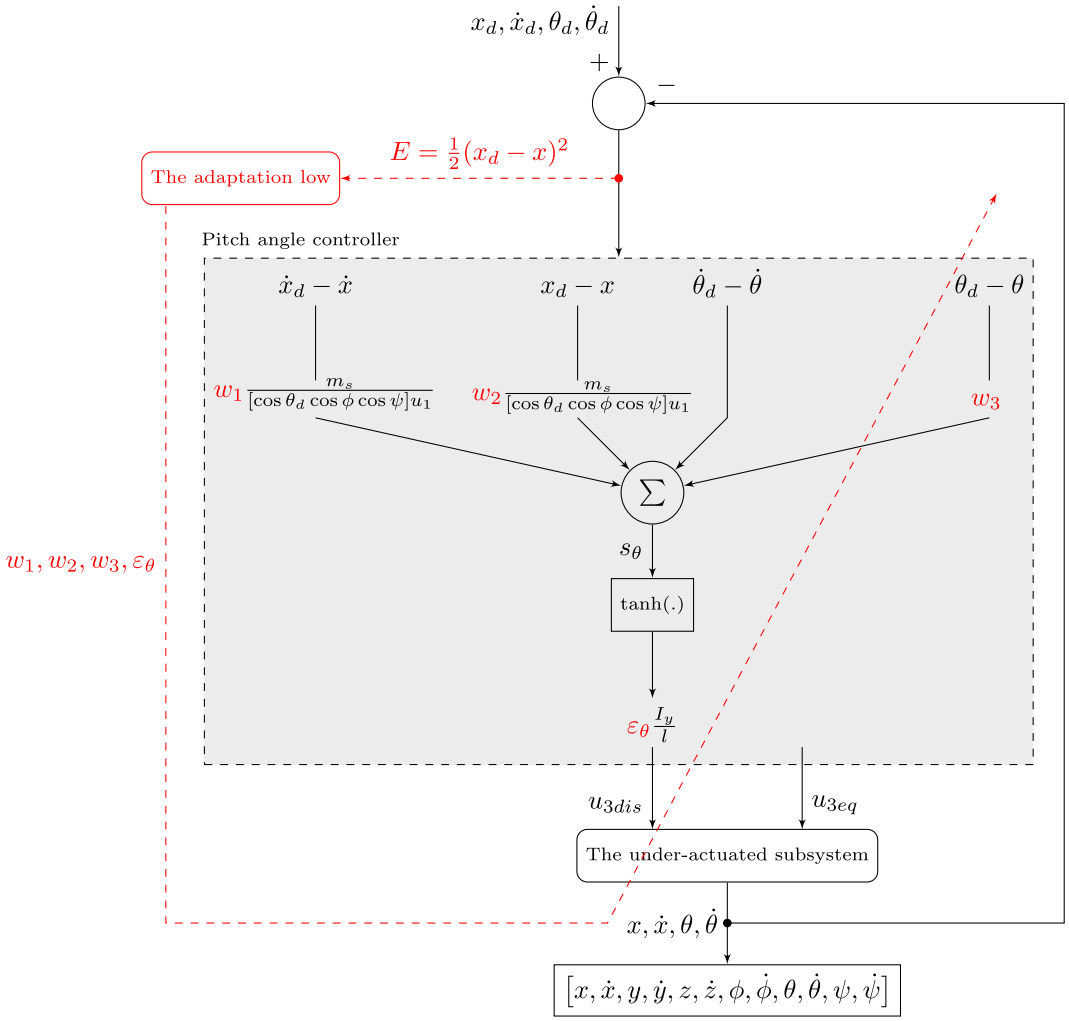


**Fig. 3.** The pitch angle controller block diagram.

$$s_\psi = w_\psi(\psi_d - \psi) + (\dot{\psi}_d - \dot{\psi}) \tag{25}$$

$$u_4 = \underbrace{\frac{I_z}{c}[w_\psi(\dot{\psi}_d - \dot{\psi}) + \ddot{\psi}_d]}_{u_{4eq}} + \underbrace{\frac{I_z}{c}[\varepsilon_\psi \tanh s_\psi]}_{u_{4dis}} \tag{26}$$

Likewise, the neural network is used to adjust the positive coefficients $w_\psi$ and $\varepsilon_\psi$, and following results are obtained:

$$\varepsilon_\psi = \varepsilon_{\psi,0} + \eta_\psi \int_0^t \text{sign}\Big(\frac{\nabla\psi}{\nabla u_{4dis}}\Big)\frac{I_z(\psi_d - \psi)\tanh s_\psi}{c}dt \tag{27}$$

$$w_\psi = w_{\psi,0} + \eta_\psi \int_0^t \text{sign}\Big(\frac{\nabla\psi}{\nabla u_{4dis}}\Big)\frac{4I_z\varepsilon_\psi(\psi_d - \psi)^2 e^{-2s_\psi}}{c(1+e^{-2s_\psi})^2}dt \tag{28}$$

The trial and error method will be used in $\eta_\psi$, $\varepsilon_{\psi,0}$ and $w_{\psi,0}$ consideration.

### 4.3. Pitch angle controller design

The objective of pitch angle controller design is to guarantee the state variables $[x, \theta]$ converge to the desired trajectories $[x_d, \theta_d]$.

In accordance with (8), the dynamic equation (5) can be expressed as follows:

$$\begin{cases} \dot{x}_9 = x_{10} \\ \dot{x}_{10} = [0] + [\frac{l}{I_y}]u_3 + [\dot{\phi}\dot{\psi}\frac{I_z - I_x}{I_y} - \frac{J_r}{I_y}\dot{\phi}\Omega_r - \frac{k_5 l}{I_y}\dot{\theta}] \end{cases} \tag{29}$$

where, $i = 9$, $j = 3$, $x_9 = \theta$, $x_{10} = \dot{\theta}$, $f(\boldsymbol{x}) = 0$, $h(\boldsymbol{x}) = \frac{l}{I_y}$, and $d(\boldsymbol{x}) = \dot{\phi}\dot{\psi}\frac{I_z - I_x}{I_y} - \frac{J_r}{I_y}\dot{\phi}\Omega_r - \frac{k_5 l}{I_y}\dot{\theta}$.

The pitch angle control problem, which is illustrated in Fig. 3, is formulated as follows.

**Step 1.** Choose the following sliding surface which is a linear combination of position and velocity tracking errors of two state variables $[x, \theta]$:

$$s_\theta = \alpha_1(\dot{x}_d - \dot{x}) + \alpha_2(x_d - x) + (\dot{\theta}_d - \dot{\theta}) + \alpha_3(\theta_d - \theta) \tag{30}$$

where, $\alpha_1$, $\alpha_2$, and $\alpha_2$ are three design constants.

The derivative of $s$ with respect to time can be obtained as follows:

$$\dot{s}_\theta = \alpha_1(\ddot{x}_d - \ddot{x}) + \alpha_2(\dot{x}_d - \dot{x}) + (\ddot{\theta}_d - \ddot{\theta}) + \alpha_3(\dot{\theta}_d - \dot{\theta}) \tag{31}$$

Substituting (1) and (5) into (31) yields:

$$\dot{s}_\theta = \alpha_1\Big(\ddot{x}_d - \frac{\sin\theta\cos\phi\cos\psi}{m_s}u_1\Big) + \alpha_2(\dot{x}_d - \dot{x}) + \Big(\ddot{\theta}_d - \frac{l}{I_y}u_3\Big) + \alpha_3(\dot{\theta}_d - \dot{\theta}) \tag{32}$$

**Step 2.** The desired asymptotic behavior in steady state of the closed-loop system is investigated as follows [35]:

Setting $s_\theta$ and $\dot{s}_\theta$ to zero, (30) and (31) is transformed to:

$$\dot{x}_d - \dot{x} = -\frac{\alpha_2}{\alpha_1}(x_d - x) - \frac{1}{\alpha_1}(\dot{\theta}_d - \dot{\theta}) - \frac{\alpha_3}{\alpha_1}(\theta_d - \theta) \tag{33}$$

$$\ddot{\theta}_d - \ddot{\theta} = -\alpha_1(\ddot{x}_d - \ddot{x}) - \alpha_2(\dot{x}_d - \dot{x}) - \alpha_3(\dot{\theta}_d - \dot{\theta}) \tag{34}$$

Assuming $\upsilon_1 = \theta_d - \theta$, $\upsilon_2 = \dot{\theta}_d - \dot{\theta}$ and $\upsilon_3 = x_d - x$ and according to (1); (33) and (34) can be rewritten as follows:

$$\begin{cases} \dot{\upsilon}_1 = \upsilon_2 \\ \dot{\upsilon}_2 = \frac{\alpha_1[\sin(\theta_d - \upsilon_1)\cos\phi\cos\psi + \sin\phi\sin\psi]u_1}{m_s} + \frac{\alpha_2\alpha_3}{\alpha_1}\upsilon_1 \\ \qquad + [\frac{\alpha_2}{\alpha_1} - \alpha_3]\upsilon_2 + \frac{\alpha_2^2}{\alpha_1}\upsilon_3 - \alpha_1\ddot{x}_d \\ \dot{\upsilon}_3 = -\frac{\alpha_3}{\alpha_1}\upsilon_1 - \frac{1}{\alpha_1}\upsilon_2 - \frac{\alpha_2}{\alpha_1}\upsilon_3 \end{cases} \tag{35}$$

Taking the first order Taylor series expansion around the equilibrium point $[\upsilon_1, \upsilon_2, \upsilon_3] = [0, 0, 0]$, the linearized form of (35) can be written as:

$$\underbrace{\begin{pmatrix} \dot{\upsilon}_1 \\ \dot{\upsilon}_2 \\ \dot{\upsilon}_3 \end{pmatrix}}_{\dot{\upsilon}} = \underbrace{\begin{pmatrix} 0 & 1 & 0 \\ -\frac{\alpha_1[\cos\theta_d\cos\phi\cos\psi]u_1}{m_s} & \frac{\alpha_2}{\alpha_1} - \alpha_3 & \frac{\alpha_2^2}{\alpha_1} \\ -\frac{\alpha_3}{\alpha_1} & -\frac{1}{\alpha_1} & -\frac{\alpha_2}{\alpha_1} \end{pmatrix}}_{A} \underbrace{\begin{pmatrix} \upsilon_1 \\ \upsilon_2 \\ \upsilon_3 \end{pmatrix}}_{\upsilon} \tag{36}$$

Supposing $\alpha_1 = \frac{w_1 m_s}{[\cos\theta_d\cos\phi\cos\psi]u_1}$, $\alpha_2 = \frac{w_2 m_s}{[\cos\theta_d\cos\phi\cos\psi]u_1}$ and $\alpha_3 = w_3$, the characteristic polynomial (36) can be obtained as follows:

$$s^3 + w_3 s^2 + w_1 s + w_2 = 0 \tag{37}$$

In accordance with the Routh–Hurwitz theorem, it is easy to show that, all the roots of the polynomial (36) have negative real parts precisely when all the coefficients $w_1$, $w_2$ and $w_3$ are positive and $w_2 < w_1 w_3$.

**Remark 5.** An autonomous system $\dot{\upsilon} = A\upsilon$, where $\upsilon(t) \in R^n$ and $A$ is an $n \times n$ matrix with real entries, has a constant solution $\upsilon(t) = 0$. This solution is asymptotically stable as $t \to \infty$ if and only if for all eigenvalues $\lambda$ of $A$, $Re(\lambda) < 0$. Use of this result in practice, in order to determine the stability of the origin for a linear system, is simplified by the Routh-Hurwitz stability theorem. The eigenvalues of a matrix are the roots of its characteristic polynomial. A polynomial in one variable with real coefficients is called a Hurwitz polynomial if the real parts of all roots are strictly negative. The Routh-Hurwitz theorem points a characterization of Hurwitz polynomials by means of an algorithm that eschews calculation of the roots.

**Step 3.** Define the following reaching law with a designed positive number $\varepsilon_\theta$:

$$\dot{s}_\theta = -\varepsilon_\theta \tanh s_\theta \tag{38}$$

**Step 4.** The control law $u_3$ is calculated as follows:

$$u_3 = \underbrace{\frac{I_y}{l}\left[\alpha_1\left(\ddot{x}_d - \frac{\sin\theta\cos\phi\cos\psi + \sin\phi\sin\psi}{m_s}u_1\right) + \alpha_2(\dot{x}_d - \dot{x}) + \ddot{\theta}_d + \alpha_3(\dot{\theta}_d - \dot{\theta})\right]}_{u_{3eq}} + \underbrace{\frac{I_y}{l}[\varepsilon_\theta \tanh s_\theta]}_{u_{3dis}} \tag{39}$$

**Step 5.** Considering the positive Lyapunov function candidate $V = \frac{1}{2}s_\theta^2$, the proof of the stability of the closed-loop system is similar to Theorem 1.

**Remark 6.** There is four design parameters, $w_1$, $w_2$, $w_3$ and $\varepsilon_\theta$ which can be selected based on the requirements for the conversion speed of discontinuous control and the steady-state tracking precision or the fastness of the sliding mode system.

**Step 6.** To adapt the coefficients $w_1$, $w_2$, $w_3$ and $\varepsilon_\theta$, neural network is trained to minimize the following error $E$:

$$E = \frac{1}{2}(x_d - x)^2 \tag{40}$$

The adaptation equations are as follows:

$$\varepsilon_\theta = \varepsilon_{\theta,0} - \eta_\theta \int_0^t \frac{\partial E}{\partial \varepsilon_\theta} dt \tag{41}$$

$$w_1 = w_{1,0} - \eta_\theta \int_0^t \frac{\partial E}{\partial w_1} dt \tag{42}$$

$$w_2 = w_{2,0} - \eta_\theta \int_0^t \frac{\partial E}{\partial w_2} dt \tag{43}$$

$$w_3 = w_{3,0} - \eta_\theta \int_0^t \frac{\partial E}{\partial w_3} dt \tag{44}$$

where, $\eta_\theta$ is the learning rate, and $\varepsilon_{\theta,0}$, $w_{1,0}$, $w_{2,0}$ and $w_{3,0}$ are the initial values of $\varepsilon_\theta$, $w_1$, $w_2$ and $w_3$, respectively and will be considered by the trial and error method.

By applying the chain rule and assuming that $\frac{\partial x}{\partial u_{3dis}} = \text{sign}\left(\frac{\nabla x}{\nabla u_{3dis}}\right)$ [33], we can formulate (41)–(44) as follows:

$$\varepsilon_\theta = \varepsilon_{\theta,0} + \eta_\theta \int_0^t \text{sign}\left(\frac{\nabla x}{\nabla u_{3dis}}\right)\frac{I_y(x_d - x)\tanh s_\theta}{l} dt \tag{45}$$

$$w_1 = w_{1,0} + \eta_\theta \int_0^t \text{sign}\left(\frac{\nabla x}{\nabla u_{3dis}}\right)\frac{4I_y m_s \varepsilon_\theta (x_d - x)(\dot{x}_d - \dot{x})e^{-2s_\theta}}{l\cos\theta_d\cos\phi\cos\psi(1 + e^{-2s_\theta})^2 u_1} dt \tag{46}$$

$$w_2 = w_{2,0} + \eta_\theta \int_0^t \text{sign}\left(\frac{\nabla x}{\nabla u_{3dis}}\right)\frac{4I_y m_s \varepsilon_\theta (x_d - x)^2 e^{-2s_\theta}}{l\cos\theta_d\cos\phi\cos\psi(1 + e^{-2s_\theta})^2 u_1} dt \tag{47}$$

$$w_3 = w_{3,0} + \eta_\theta \int_0^t \text{sign}\left(\frac{\nabla x}{\nabla u_{3dis}}\right)\frac{4I_y \varepsilon_\theta (x_d - x)(\theta_d - \theta)e^{-2s_\theta}}{l(1 + e^{-2s_\theta})^2} dt \tag{48}$$

### 4.4. Roll angle controller design

The roll angle controller must be designed so that the state variables $[y, \phi]$ can track the desire variables $[y_d, \phi_d]$. We have the following dynamical equations required for this subsystem:

$$\begin{cases} \dot{x}_7 = x_8 \\ \dot{x}_8 = [0] + [\frac{l}{I_x}]u_2 + [\dot{\theta}\dot{\psi}\frac{I_y - I_z}{I_x} + \frac{J_r}{I_x}\dot{\theta}\Omega_r - \frac{k_4 l}{I_x}\dot{\phi}] \end{cases} \tag{49}$$

where, $i = 7$, $j = 2$, $x_7 = \phi$, $x_8 = \dot{\phi}$, $f(\boldsymbol{x}) = 0$, $h(\boldsymbol{x}) = \frac{l}{I_x}$, and $d(\boldsymbol{x}) = \dot{\theta}\dot{\psi}\frac{I_y - I_z}{I_x} + \frac{J_r}{I_x}\dot{\theta}\Omega_r - \frac{k_4 l}{I_x}\dot{\phi}$.

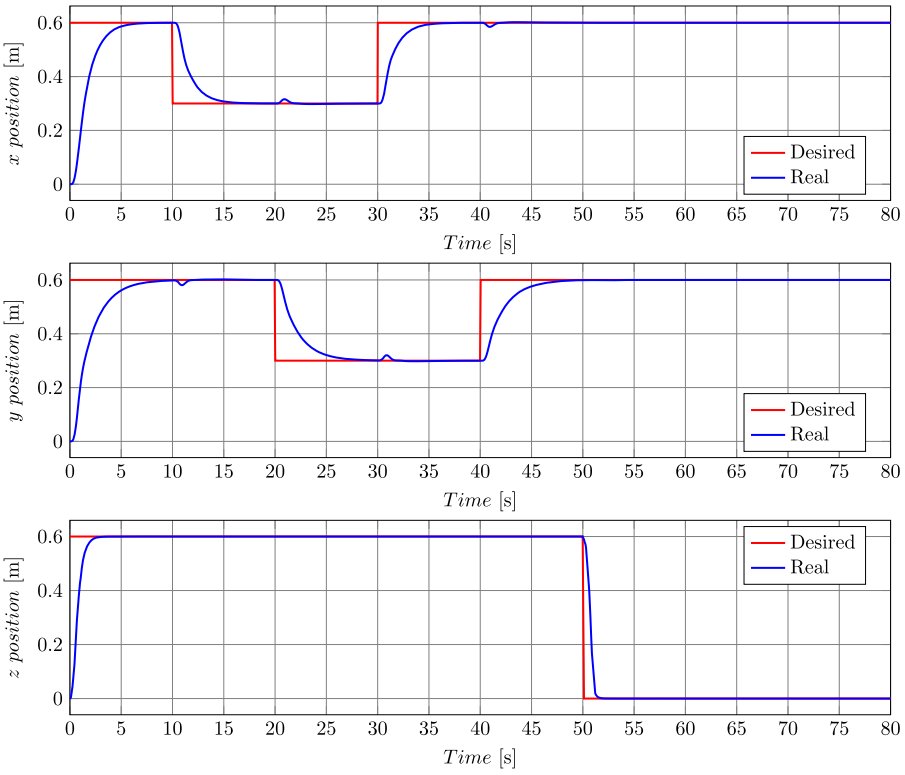


**Fig. 4.** Position tracking results.

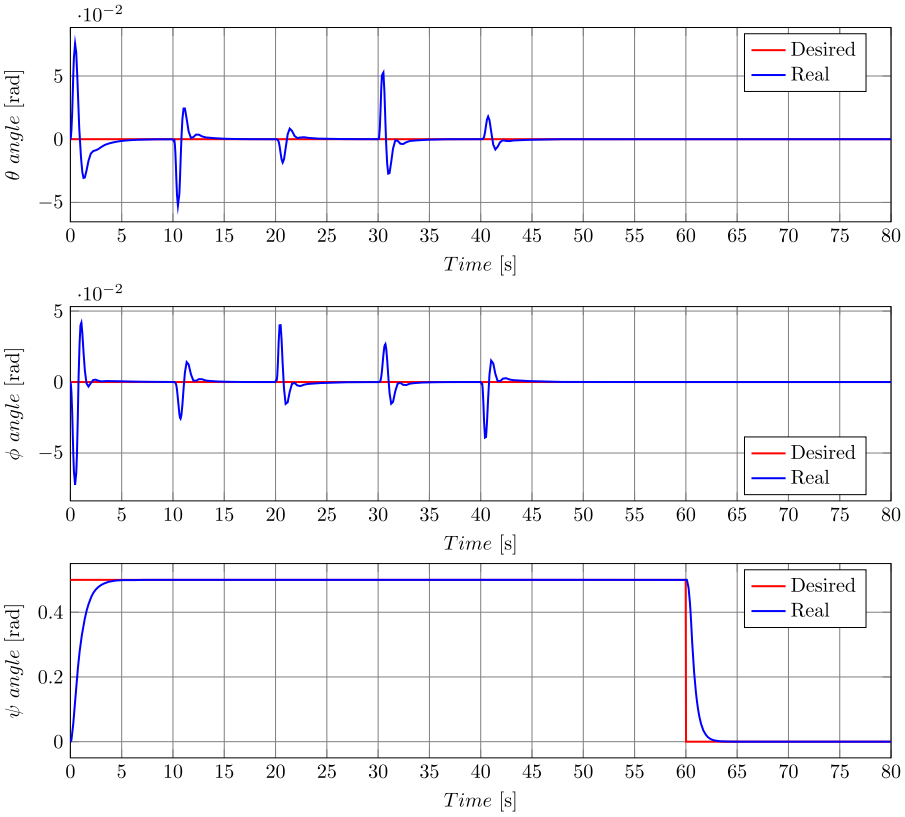


**Fig. 5.** Attitude tracking results.

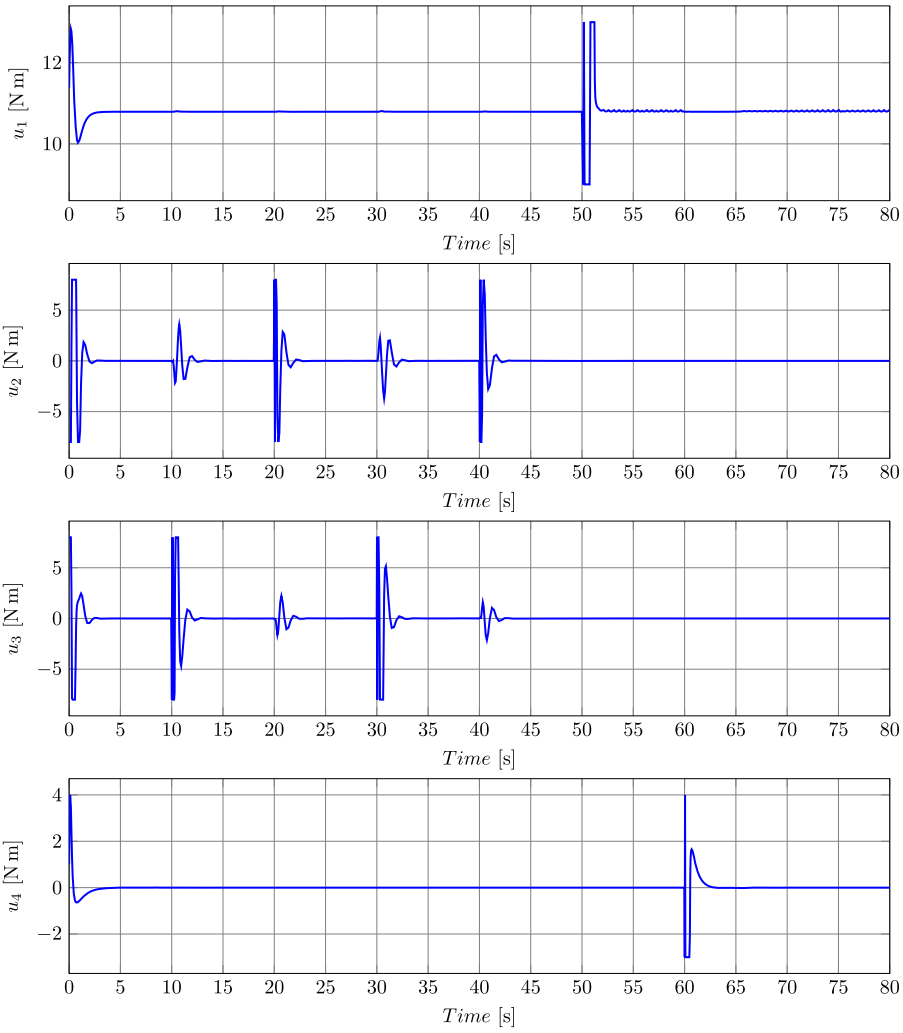


**Fig. 6.** Control inputs.

Similar to the pitch angle control, we have the following sliding surface and control input $s_\phi$ and $u_2$:

$$s_\phi = \alpha_4(\dot{y}_d - \dot{y}) + \alpha_5(y_d - y) + (\dot{\phi}_d - \dot{\phi}) + \alpha_6(\phi_d - \phi) \tag{50}$$

$$u_2 = \underbrace{\frac{I_x}{l}\Big[\alpha_4\Big(\ddot{y}_d - \frac{\sin\theta\cos\phi\sin\psi - \sin\phi\cos\psi}{m_s}u_1\Big) + \alpha_5(\dot{y}_d - \dot{y}) + \ddot{\phi}_d + \alpha_6(\dot{\phi}_d - \dot{\phi})\Big]}_{u_{2eq}} + \underbrace{\frac{I_x}{l}[\varepsilon_\phi \tanh s_\phi]}_{u_{2dis}} \tag{51}$$

It is supposed that:

$$\alpha_4 = -\frac{w_4 m_s}{[\sin\theta\sin\phi_d\sin\psi - \cos\phi_d\cos\psi]u_1} \tag{52}$$

$$\alpha_5 = -\frac{w_5 m_s}{[\sin\theta\sin\phi_d\sin\psi - \cos\phi_d\cos\psi]u_1} \tag{53}$$

$$\alpha_6 = w_6 \tag{54}$$

Using Routh-Hurwitz criteria, the desired asymptotic behavior in steady state of the linearized closed-loop system can be achieved when $w_4$, $w_5$ and $w_6$ are positive and $w_5 < w_4 w_6$.

Similarly, the following results are obtained by using the neural network:

$$\varepsilon_\phi = \varepsilon_{\phi,0} + \eta_\phi \int_0^t \operatorname{sign}\Big(\frac{\nabla y}{\nabla u_{2dis}}\Big)\frac{I_x(y_d - y)\tanh s_\phi}{l}dt \tag{55}$$

$$w_4 = w_{4,0} - \eta_\phi \int_0^t \operatorname{sign}\Big(\frac{\nabla y}{\nabla u_{2dis}}\Big) \times \frac{4I_x m_s \varepsilon_\phi (y_d - y)(\dot{y}_d - \dot{y})e^{-2s_\phi}}{l[\sin\theta\sin\phi_d\sin\psi + \cos\phi_d\cos\psi](1 + e^{-2s_\phi})^2 u_1}dt \tag{56}$$

$$w_5 = w_{5,0} - \eta_\phi \int_0^t \operatorname{sign}\Big(\frac{\nabla y}{\nabla u_{2dis}}\Big) \times \frac{4I_x m_s \varepsilon_\phi (y_d - y)^2 e^{-2s_\phi}}{l[\sin\theta\sin\phi_d\sin\psi + \cos\phi_d\cos\psi](1 + e^{-2s_\phi})^2 u_1}dt \tag{57}$$

$$w_6 = w_{6,0} + \eta_\phi \int_0^t \operatorname{sign}\Big(\frac{\nabla y}{\nabla u_{2dis}}\Big)\frac{4I_x\varepsilon_\phi(y_d - y)(\phi_d - \phi)e^{-2s_\phi}}{l(1 + e^{-2s_\phi})^2}dt \tag{58}$$

The values of parameters $\eta_\phi$, $w_{4,0}$, $w_{5,0}$ and $w_{6,0}$ will be obtained by the trial and error method.

In the next section, the results of employing the proposed controller in the position and attitude control of a quadrotor UAV in different situations are evaluated and compared with other methods.

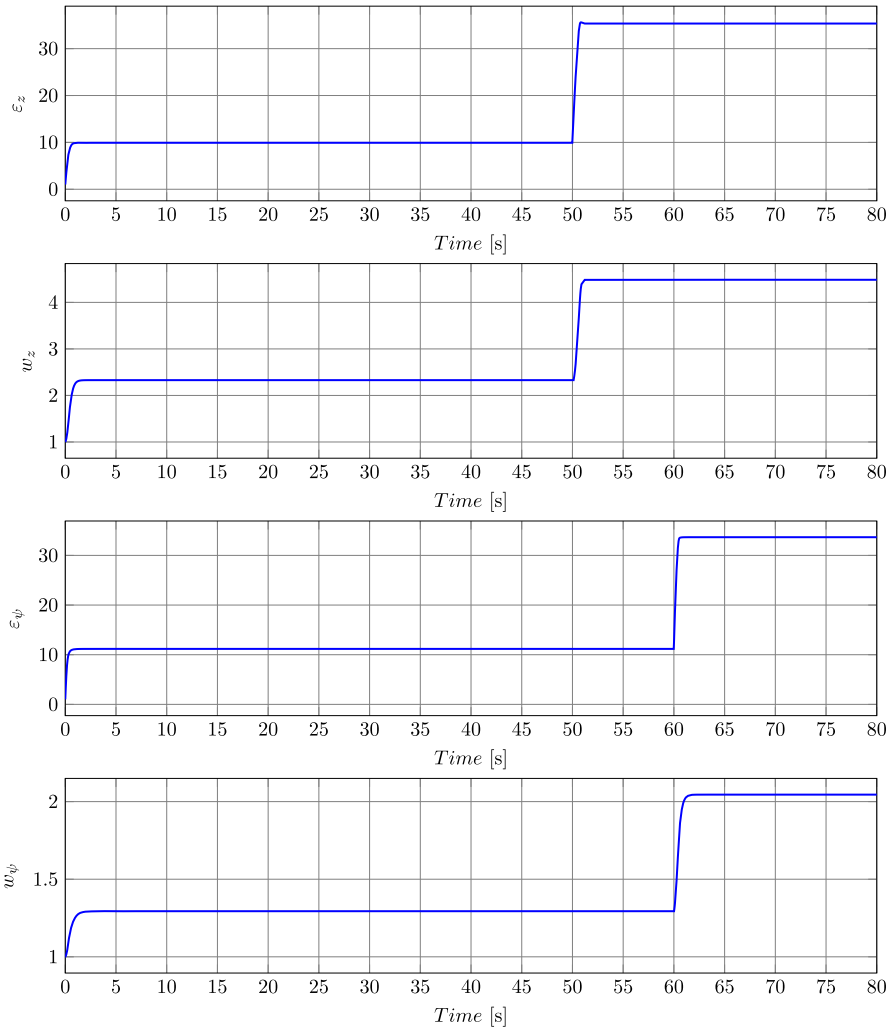


**Fig. 7.** Adjustable parameters for controllers $u_1$ and $u_4$.

**Table 1**
The numerical values of quadrotor UAV model parameters.

| Parameter | Value | Unit |
|---|---|---|
| $m_s$ | 1.1 | [kg] |
| $l$ | 0.21 | [m] |
| $I_x$ | 1.22 | [Ns$^2$/rad] |
| $I_y$ | 1.22 | [Ns$^2$/rad] |
| $I_z$ | 2.2 | [Ns$^2$/rad] |
| $J_r$ | 0.2 | [Ns$^2$/rad] |
| $k_i$ ($i=1,\ 2,\ and\ 3$) | 0.1 | [Ns/m] |
| $k_i$ ($i=4,\ 5,\ and\ 6$) | 0.12 | [Ns/m] |
| $g$ | 9.81 | [m/s$^2$] |
| $b$ | 5 | [N m$^2$] |
| $k$ | 2 | [N/ms$^2$] |
| $c$ | 1 | – |

**Table 2**
The numerical values of controller parameters.

| Parameter | Value | Parameter | Value |
|---|---|---|---|
| $\varepsilon_{z,0}$ | 1 | $w_{z,0}$ | 1 |
| $\varepsilon_{\psi,0}$ | 1 | $w_{\psi,0}$ | 1 |
| $\varepsilon_{\theta,0}$ | 10 | $w_{1,0}$ | 40 |
| $\varepsilon_{\phi,0}$ | 7.5 | $w_{2,0}$ | 25 |
| $\eta_z$ | 1 | $w_{3,0}$ | 10 |
| $\eta_\psi$ | 0.1 | $w_{4,0}$ | 40 |
| $\eta_\theta$ | 1 | $w_{5,0}$ | 25 |
| $\eta_\phi$ | 1 | $w_{6,0}$ | 10 |

## 5. Simulation results

In this section, the performance of the proposed controller is evaluated in the presence of parametric uncertainties and disturbances by simulation in the MATLAB/Simulink software. The values of the quadrotor UAV model and proposed controller parameters are summarized in Tables 1 and 2, respectively. It is obvious that the results will change by taking into account other numerical values for these parameters.

The purpose of the controller design is to track the following desired trajectory:

$$
\begin{aligned}
x_d &= \begin{cases} 0.6, & \text{if } t \le 10 \text{ or } t > 30; \\ 0.3, & \text{otherwise.} \end{cases}; \\
z_d &= \begin{cases} 0.6, & \text{if } t \le 50; \\ 0, & \text{otherwise.} \end{cases}; \quad \theta_d = 0 \\
y_d &= \begin{cases} 0.6, & \text{if } t \le 20 \text{ or } t > 40; \\ 0.3, & \text{otherwise.} \end{cases}; \\
\psi_d &= \begin{cases} 0.5, & \text{if } t \le 60; \\ 0, & \text{otherwise.} \end{cases}; \quad \phi_d = 0
\end{aligned}
\tag{59}
$$

Simulations are presented in the following subsections.

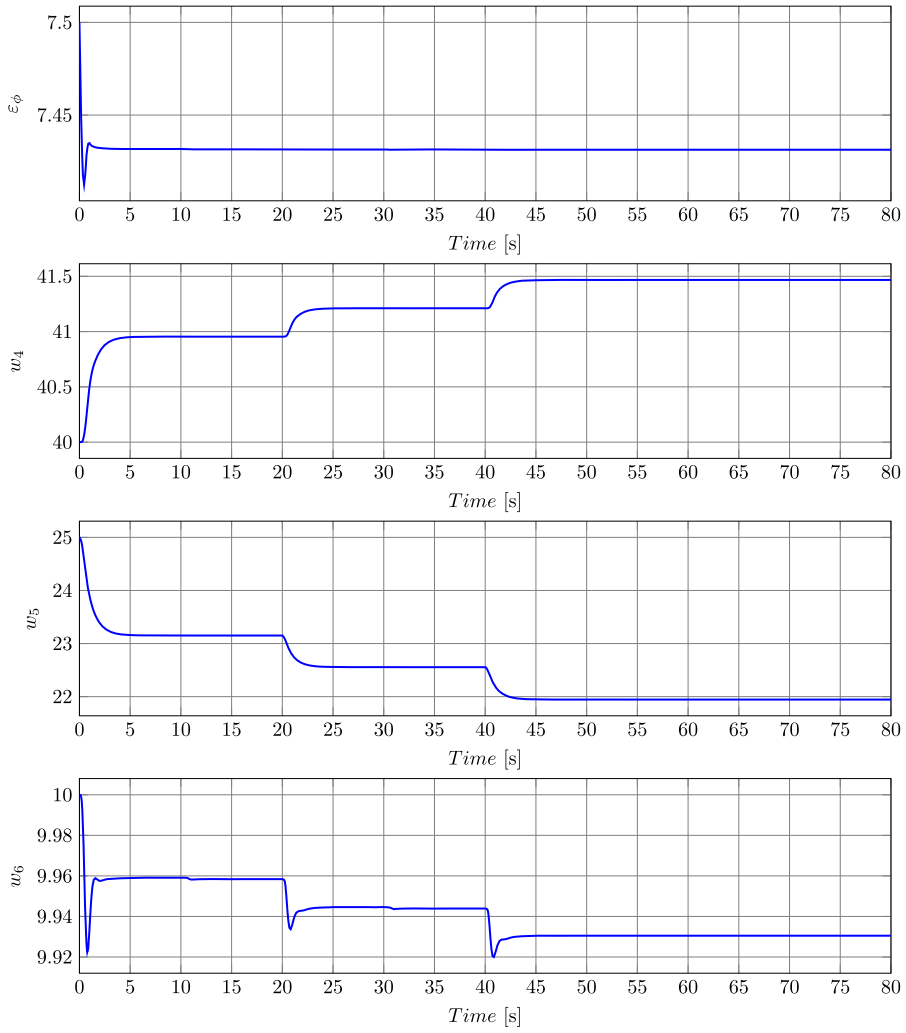


**Fig. 8.** Adjustable parameters for controller $u_2$.

### 5.1. Desired trajectory tracking with parametric and unstructured uncertainties

In this subsection, the following assumptions have been made:

- The initial values of state variables are assumed to be zero.
- $d(x)$ term, which is a not-modeled dynamic part, is neglected in the controller design in order to consider unstructured uncertainty.
- In the numerical values of $I_x$, $I_y$, $I_z$, $l$, and $c$ parameters, 25% of uncertainty is considered.

Tracking the variables $x$, $y$ and $z$ are shown in Fig. 4 and that of the variables $\theta$, $\phi$ and $\psi$ in Fig. 5. Although the selected desired trajectory has sudden changes, tracking has been done with reasonable accuracy. As shown in Figs. 4 and 5, the percentage of maximum overshoot is very small in tracking variables $x$, $y$, $z$ and $\psi$. However, in spite of considering parametric and unstructured uncertainties, the steady state error in tracking these variables is equal to zero. Control inputs $u_1$ through $u_4$ are also shown in Fig. 6. In none of the control signals there is undesired chattering phenomenon. The adjustable parameters of the controllers $u_1$ and $u_4$ in Fig. 7 and the controllers $u_2$ and $u_3$ are shown in Figs. 8 and 9, respectively. Also, the time histories of sliding mode have been shown in Fig. 10. From Fig. 10, it can be observed that all the sliding surfaces attenuate gradually and converge to the neighborhood of zero asymptotically.

Fig. 11 compares the performance of the proposed methods in this paper and references [11] and [13] in tracking the desired trajectory in 3D space. It should be noted that the proposed method in reference [13] has not been simulated; however, given the very similarity of the results presented in this reference with reference [11], both references are pointed in Fig. 11. As shown in Fig. 11, the performance of our proposed controller is better than the proposed methods in the other two mentioned references. For better comparison of these methods, the numerical results of the maximum overshoot, settling time and steady state error are compared in Table 3. According to the numerical results of Table 3, in the following cases, the controller performance proposed in this paper is superior to the method presented in reference [11]:

- It has 43.75% and 28.55% lower maximum overshoot in tracking variables $x$ and $y$, respectively.
- It has 3.18%, 11.09%, 50.46% and 23.32% lower settling time in tracking variables $x$, $y$, $z$ and $\psi$, respectively.

### 5.2. Desired trajectory tracking with external disturbances

In this subsection, in addition to the assumptions in the previous subsection, the term $0.01\sin(0.01t)$ is added as the external

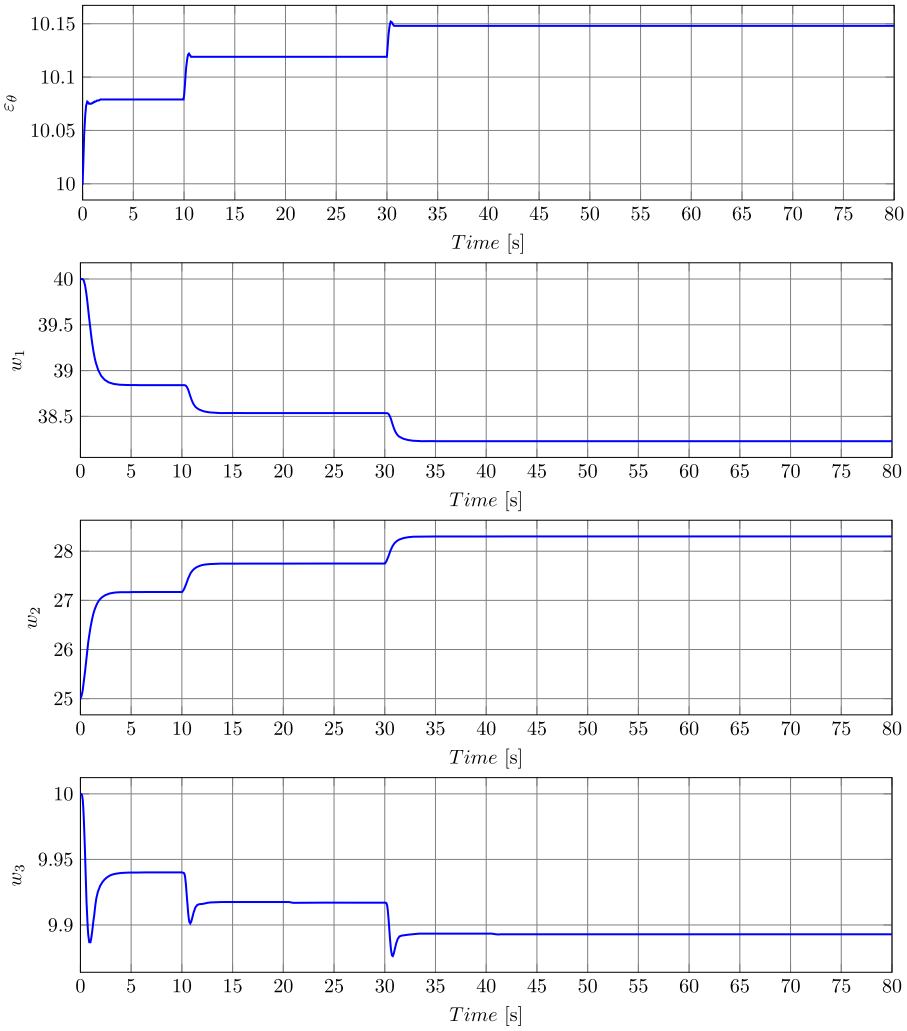


**Fig. 9.** Adjustable parameters for controller $u_3$.

**Table 3**
Quantitative comparisons of simulation results.

| | | The proposed method in this article | The method presented in the reference [11] |
|---|---|---|---|
| Maximum overshoot [%] | $x$ | 5.2658 | 9.3612 |
| | $y$ | 6.8057 | 9.5251 |
| | $z$ | $3.2255 \times 10^{-8}$ | 0.0109 |
| | $\psi$ | 0.0038 | 0.0101 |
| Settling time [s] | $x$ | 4.2947 | 4.4357 |
| | $y$ | 5.4823 | 6.1658 |
| | $z$ | 1.7629 | 3.5583 |
| | $\psi$ | 2.7284 | 3.5583 |
| Steady state error | $x$ [m] | $6.8834 \times 10^{-14}$ | $1.9382 \times 10^{-6}$ |
| | $y$ [m] | $1.1996 \times 10^{-10}$ | $3.2554 \times 10^{-6}$ |
| | $z$ [m] | $2.9662 \times 10^{-5}$ | $1.9369 \times 10^{-8}$ |
| | $\psi$ [rad] | $1.0738 \times 10^{-16}$ | $2.0552 \times 10^{-4}$ |

disturbance to the right of Eqs. (1)–(6). Also, 5% uncertainty in the value of parameter $m_s$ is considered.

Fig. 12 compares the performance of the controllers proposed in this paper and reference [11] in tracking variables $x$, $y$, $z$ and $\psi$. Also, the trajectory tracking results obtained from using the methods presented in this article and Reference [11] in 3D are shown in Fig. 13. As shown in Figs. 12 and 13, the controller proposed in reference [11] is not robust to the uncertainty of the $m_s$ parameter, and this uncertainty leads to a steady state error in tracking variable $z$.

Quantitative comparisons of trajectory tracking results are given in Table 4 and the proposed controller shows better performance compared to the controller proposed in reference [11]. The results of this table are summarized below:

- Using the proposed method in this article instead of the controller proposed in reference [11] causes 12.29, 5.51, 50.14 and 30.89 percent less settling time to track variables $x$, $y$, $z$ and $\psi$, respectively.

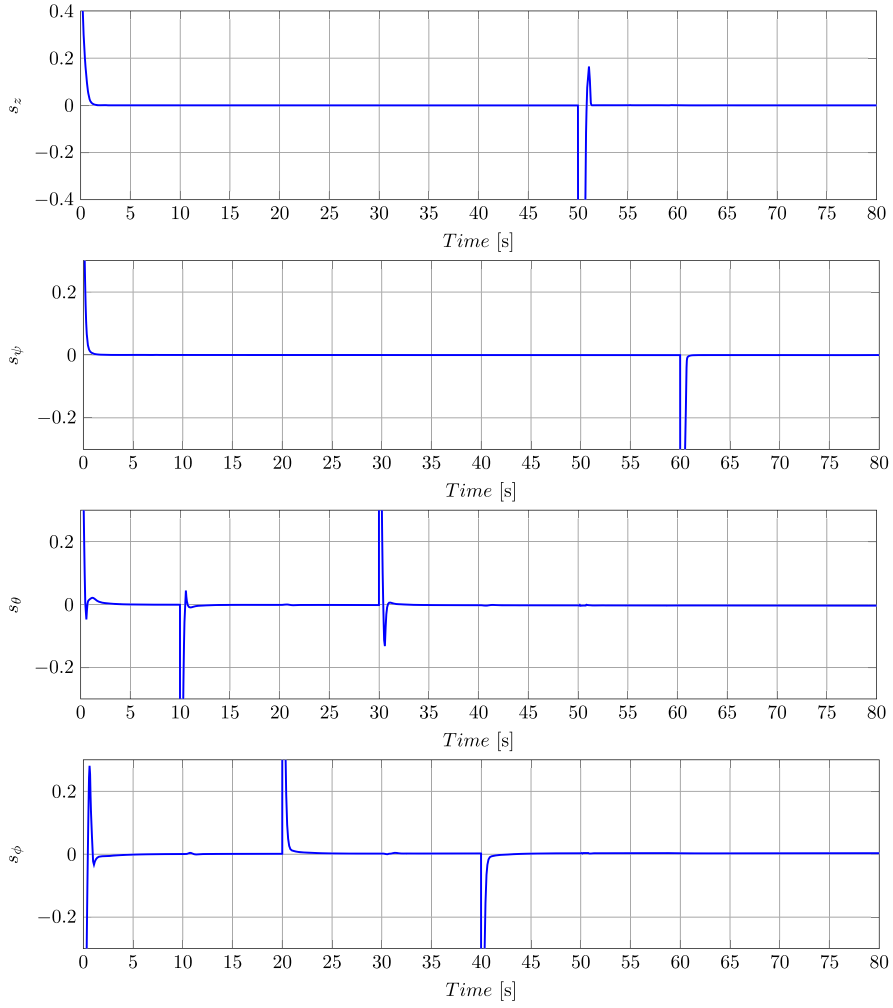


**Fig. 10.** The sliding variables.

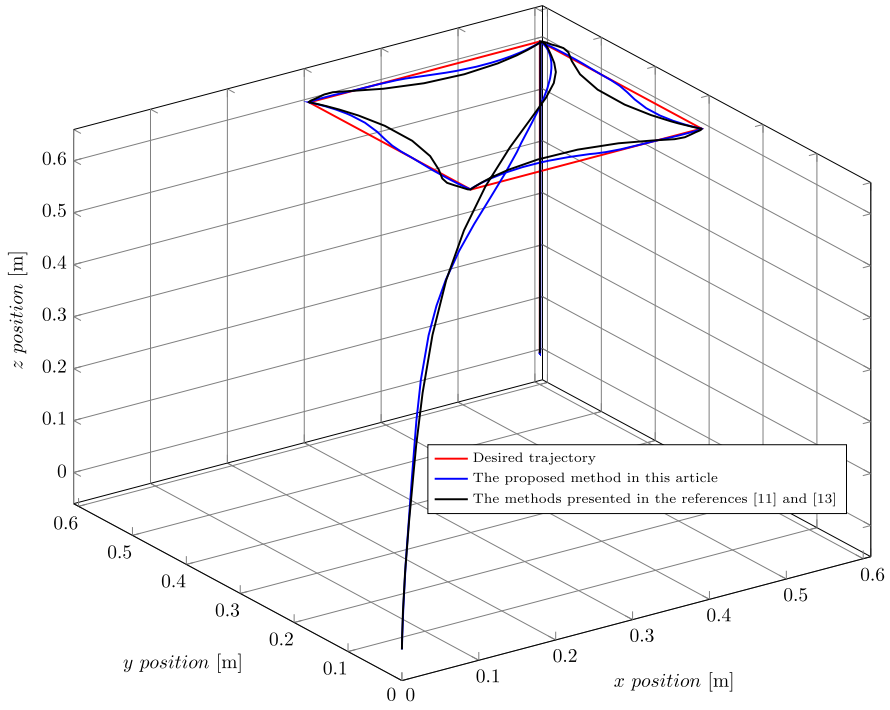


**Fig. 11.** Quarotor's path.

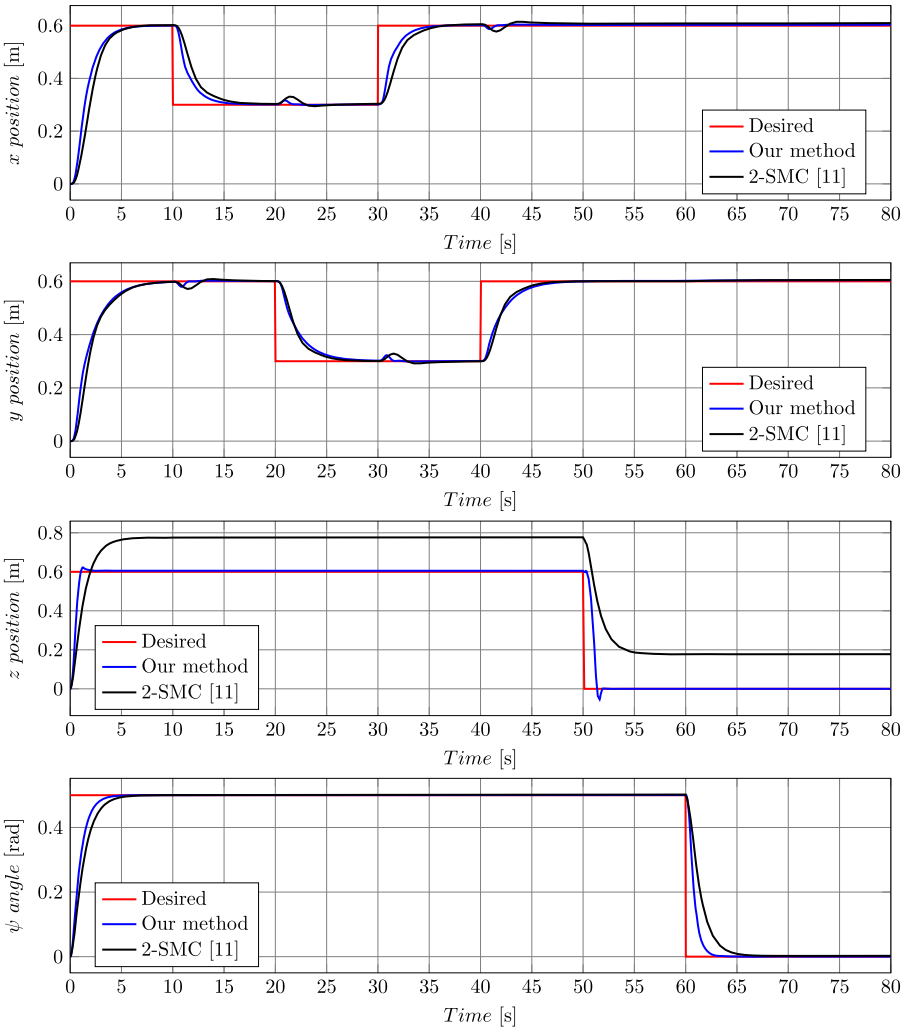


**Fig. 12.** Compare tracking results.

**Table 4**
Quantitative comparisons of simulation results.

| | | The proposed method in this article | The method presented in the reference [11] |
|---|---|---|---|
| Maximum overshoot [%] | $x$ | 5.6833 | 10.2499 |
| | $y$ | 7.5133 | 9.5647 |
| | $z$ | 3.7433 | 0 |
| | $\psi$ | 0.0120 | 0.0515 |
| Settling time [s] | $x$ | 4.1946 | 4.7822 |
| | $y$ | 5.6648 | 5.9952 |
| | $z$ | 0.9826 | 1.9708 |
| | $\psi$ | 2.6486 | 3.8325 |
| Steady state error | $x$ [m] | 0.0034 | 0.0097 |
| | $y$ [m] | 0.0044 | 0.0052 |
| | $z$ [m] | $8.0761 \times 10^{-5}$ | 0.1776 |
| | $\psi$ [rad] | $1.2532 \times 10^{-4}$ | 0.0025 |

- In comparison with the method presented in reference [11], the use of the controller proposed in this paper for the tracking of the variables $x$ and $y$, shows 44.55 and 21.45 percent decrease in maximum overshoot, respectively.
- When using the method proposed in this article, the variable $z$ is tracked with a settling time of 0.9826 s, a maximum overshoot of 3.7433% and without the steady state error, while using the method presented in reference [11], this variable will be tracked with a settling time of 1.9708 s, a maximum overshoot of 0% and the steady state error of 0.1776 m.

As a result, the proposed method in this paper trackes the desired trajectory with acceptable transient and steady state response characteristics, and provides robustness against parametric uncertainties and external disturbances.

## 6. Conclusion

In this paper, the position and attitude tracking of a quadrotor UAV by using an adaptive sliding mode control was investigated. In order to improve the proposed control method efficiency, a neural

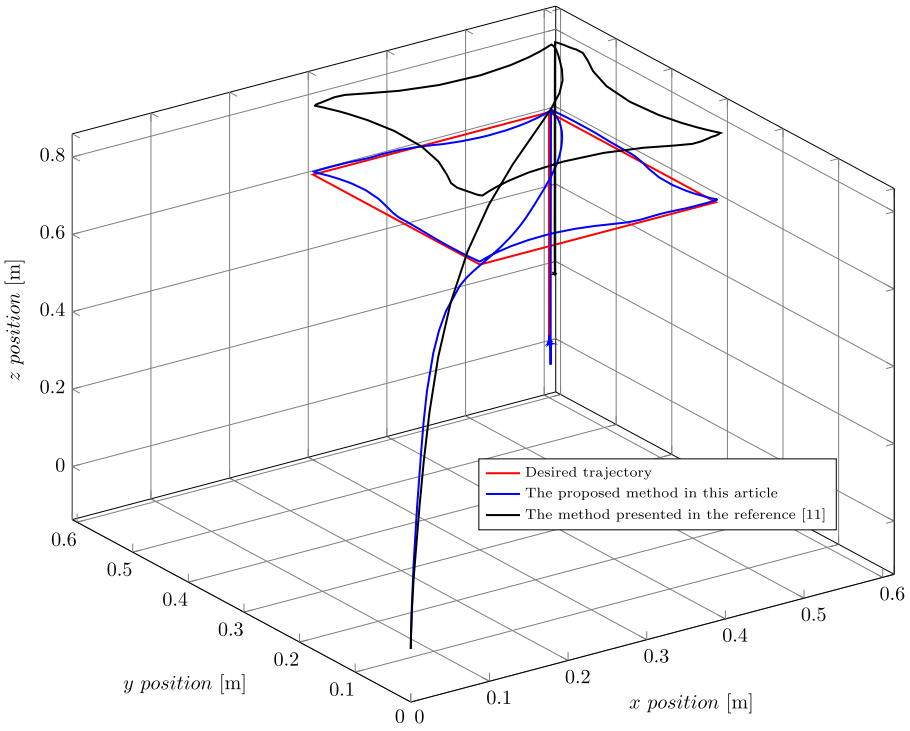


**Fig. 13.** Quarotor's path.

network was applied to adjust the sliding mode controller parameters, adaptively. A specialized learning architecture based on some approximation of the backpropagated error that allows adaptive control with a neural network was proposed. The performance of the adaptive sliding mode control method in the tracking purposes of a quadrotor UAV in the presence of parametric uncertainties and external disturbance was presented. Moreover, the results of the position and attitude tracking by means of our proposed method and the methods proposed in references [11] and [13] were compared. The proposed adaptive sliding mode control method has the advantages of higher speed and accuracy, less sensitivity to parameter variations and disturbances, and the chattering avoidance in the control inputs and the obtained results confirm the integrity of this approach.

## Declaration of Competing Interest

None declared under financial, general, and institutional competing interests.

## Acknowledgements

The authors are thankful to authorities of East Tehran Branch, Islamic Azad University, Tehran, Iran, for providing support and necessary facilities.

## References

[1] B. Tian, L. Liu, H. Lu, Z. Zuo, Q. Zong, Y. Zhang, Multivariable finite time attitude control for quadrotor UAV: theory and experimentation, IEEE Trans. Ind. Electron. 65 (3) (2018) 2567–2577.
[2] H. Du, W. Zhu, G. Wen, D. Wu, Finite-time formation control for a group of quadrotor aircraft, Aerosp. Sci. Technol. 69 (2017) 609–616.
[3] X. Liang, Y. Fang, N. Sun, H. Lin, Nonlinear hierarchical control for unmanned quadrotor transportation systems, IEEE Trans. Ind. Electron. 65 (4) (2018) 3395–3405.
[4] Y.C. Choi, H.S. Ahn, Nonlinear control of quadrotor for point tracking: actual implementation and experimental tests, IEEE/ASME Trans. Mechatron. 20 (3) (2015) 1179–1192.
[5] Z. Jia, J. Yu, Y. Mei, Y. Chen, Y. Shen, X. Ai, Integral backstepping sliding mode control for quadrotor helicopter under external uncertain disturbances, Aerosp. Sci. Technol. 68 (2017) 299–307.
[6] Z. Xu, X. Nian, H. Wang, Y. Chen, Robust guaranteed cost tracking control of quadrotor UAV with uncertainties, ISA Trans. 69 (2017) 157–165.
[7] R. Pérez-Alcocer, J. Moreno-Valenzuela, R. Miranda-Colorado, A robust approach for trajectory tracking control of a quadrotor with experimental validation, ISA Trans. 65 (2016) 262–274.
[8] O. Mofid, S. Mobayen, Adaptive sliding mode control for finite-time stability of quad-rotor UAVs with parametric uncertainties, ISA Trans. 72 (2018) 1–14.
[9] A. Zulu, S. John, A review of control algorithms for autonomous quadrotors, Open J. Appl. Sci. 4 (2014) 547–556.
[10] S.B.F. Asl, S.S. Moosapour, Adaptive backstepping fast terminal sliding mode controller design for ducted fan engine of thrust-vectored aircraft, Aerosp. Sci. Technol. 71 (2017) 521–529.
[11] E.H. Zheng, J.J. Xiong, J.L. Luo, Second order sliding mode control for a quadrotor UAV, ISA Trans. 53 (4) (2014) 1350–1356.
[12] Y. Yang, Y. Yan, Attitude regulation for unmanned quadrotors using adaptive fuzzy gain-scheduling sliding mode control, Aerosp. Sci. Technol. 54 (2016) 208–217.
[13] J.J. Xiong, G.B. Zhang, Global fast dynamic terminal sliding mode control for a quadrotor UAV, ISA Trans. 66 (2017) 233–240.
[14] J.J. Xiong, E.H. Zheng, Position and attitude tracking control for a quadrotor UAV, ISA Trans. 53 (3) (2014) 725–731.
[15] B. Sumantri, N. Uchiyama, S. Sano, Least square based sliding mode control for a quad-rotor helicopter and energy saving by chattering reduction, Mech. Syst. Signal Process. 66 (2016) 769–784.
[16] S. Mondal, C. Mahanta, Chattering free adaptive multivariable sliding mode controller for systems with matched and mismatched uncertainty, ISA Trans. 52 (3) (2013) 335–341.
[17] S. Zeghlache, D. Saigaa, K. Kara, Fault tolerant control based on neural network interval type-2 fuzzy sliding mode controller for octorotor UAV, Front. Comput. Sci. 10 (4) (2016) 657–672.
[18] S. Zeghlache, K. Kara, D. Saigaa, Fault tolerant control based on interval type-2 fuzzy sliding mode controller for coaxial trirotor aircraft, ISA Trans. 59 (2015) 215–231.
[19] F. Muñoz, I. González-Hernández, S. Salazar, E.S. Espinoza, R. Lozano, Second order sliding mode controllers for altitude control of a quadrotor UAS: real-time implementation in outdoor environments, Neurocomputing 233 (2017) 61–71.
[20] S. Li, Y. Wang, J. Tan, Y. Zheng, Adaptive RBFNNs/integral sliding mode control for a quadrotor aircraft, Neurocomputing 216 (2016) 126–134.
[21] I. González, S. Salazar, R. Lozano, Chattering-free sliding mode altitude control for a quad-rotor aircraft: real-time application, J. Intell. Robot. Syst. 73 (1–4) (2014) 137–155.

[22] H. Ramirez-Rodriguez, V. Parra-Vega, A. Sanchez-Orta, O. Garcia-Salazar, Robust backstepping control based on integral sliding modes for tracking of quadrotors, J. Intell. Robot. Syst. 73 (1–4) (2014) 51–66.
[23] E. Zheng, J. Xiong, Quad-rotor unmanned helicopter control via novel robust terminal sliding mode controller and under-actuated system sliding mode controller, Optik, Int. J. Light Electron Opt. 125 (12) (2014) 2817–2825.
[24] F. Chen, R. Jiang, K. Zhang, B. Jiang, G. Tao, Robust backstepping sliding-mode control and observer-based fault estimation for a quadrotor UAV, IEEE Trans. Ind. Electron. 63 (8) (2016) 5044–5056.
[25] S. Tokat, I. Eksin, M. Güzelkaya, New approaches for on-line tuning of the linear sliding surface slope in sliding mode controllers, Turk. J. Electr. Eng. Comput. Sci. 11 (1) (2003) 45–60.
[26] Y. Yueneng, Y. Ye, Backstepping sliding mode control for uncertain strict-feedback nonlinear systems using neural-network-based adaptive gain scheduling, J. Syst. Eng. Electron. 29 (3) (2018) 580–586.
[27] Y.n. Yang, J. Wu, W. Zheng, Trajectory tracking for an autonomous airship using fuzzy adaptive sliding mode control, J. Zhejiang Univ. Sci. C 13 (7) (2012) 534–543.
[28] Y. Yang, Y. Yan, Neural network approximation-based nonsingular terminal sliding mode control for trajectory tracking of robotic airships, Aerosp. Sci. Technol. 54 (2016) 192–197.
[29] Y. Yang, A time-specified nonsingular terminal sliding mode control approach for trajectory tracking of robotic airships, Nonlinear Dyn. 92 (3) (2018) 1359–1367.
[30] H. Razmi, A.M. Kashtiban, Nonlinear PID-based analog neural network control for a two link rigid robot manipulator and determining the maximum load carrying capacity, Int. J. Soft Comput. Eng. 2 (1) (2012) 228–234.
[31] M. Khalid, S. Omatu, A neural network controller for a temperature control system, IEEE Control Syst. 12 (3) (1992) 58–64.
[32] J. Ye, Adaptive control of nonlinear PID-based analog neural networks for a nonholonomic mobile robot, Neurocomputing 71 (7–9) (2008) 1561–1565.
[33] M. Saerens, A. Soquet, Neural controller based on back-propagation algorithm, in: IEE Proceedings F (Radar and Signal Processing), vol. 138, IET, 1991, pp. 55–62.
[34] H. Razmi, Adaptive neural network based sliding mode altitude control for a quadrotor UAV, J. Cent. South Univ. 25 (11) (2018) 2654–2663.
[35] N. Chatrenour, H. Razmi, H. Doagou-Mojarrad, Improved double integral sliding mode MPPT controller based parameter estimation for a stand-alone photovoltaic system, Energy Convers. Manag. 139 (2017) 97–109.